THE FIRST TWO YEARS OF IMAGE

J. L. BURCH
Southwest Research Institute
San Antonio, TX 78228-0510, U.S.A.

Abstract. The Imager for Magnetopause-to-Aurora Global Exploration (IMAGE) is the first satellite mission that is dedicated to imaging the Earth's magnetosphere. Using advanced multispectral imaging techniques along with omnidirectional radio sounding, IMAGE has provided the first glimpses into the global structure and behavior of plasmas in the inner magnetosphere. Scientific results from the two-year prime mission include the confirmation of the theory of plasmaspheric tails and the discovery of several new and unpredicted features of the plasmasphere. Neutral-atom imaging has shown how the ring current develops during magnetic storms and how ionospheric ions are injected into the ring current during substorms. The first global imaging of proton auroras has allowed the identification of the ionospheric footprint of the polar cusp and its response to changes in the interplanetary magnetic field. Detached subauroral proton arcs have been found to appear in the afternoon sector following south-north and east-west rotations of the IMF. Low-energy neutral atom imaging has shown global-scale ionospheric outflow to be an immediate response to solar-wind pressure pulses. Such imaging has also provided the first measurements of solar wind and interstellar neutral atoms from inside the magnetosphere. Radio sounding has revealed the internal structure of the plasmasphere and identified plasma cavities as the source of kilometric continuum radiation. These and numerous other scientific results now set the stage for the extended mission of IMAGE in which the imaging perspective will change markedly owing to orbital evolution while the magnetospheric environment undergoes a transition from solar maximum toward solar minimum.

1. Introduction

IMAGE is the first satellite mission dedicated to imaging the Earth's magnetosphere and is the first mission to achieve global multispectral imaging of magnetospheric plasmas with time scales relevant to the development of substorms (Burch, 2000). The overall science objective of IMAGE is to determine the response of the Earth's magnetosphere to changing conditions in the solar wind. IMAGE addresses this objective by seeking the answers to three specific science questions: 1. What are the dominant mechanisms for injecting plasma into the magnetosphere on substorm and magnetic storm time scales? 2. What is the directly driven response of the magnetosphere to solar wind changes? and 3. How and where are plasmas energized, transported, and subsequently lost during storms and substorms?

Table I lists the six imaging instruments that were designed to address these questions. The new imaging techniques include ultraviolet detection of helium ions and energetic hydrogen atoms; neutral atom imaging in three different energy ranges that encompass ionospheric outflow, solar-wind injection, and trapped

Space Science Reviews **109:** 1–24, 2003.

TABLE I
IMAGE Science Instruments

Imager	Lead Investigator	Objectives	Measurements
LENA	Thomas E. Moore NASA/GSFC	Image Ionospheric outflow.	Neutral atom composition and flux at 10 eV to 1 keV with field of view of 90° x 360°, angular resolution of 8°, and energy resolution of 80%
MENA	Craig J. Pollock Southwest Research Institute	Image inner region of plasma sheet.	Neutral atom composition and flux at 1 keV to 50 keV with field of view of 90° × 120°, angular resolution of 8°, and energy resolution of 80%
HENA	Donald G. Mitchell Johns Hopkins Univ., Applied Physics Laboratory	Image ring current.	Neutral atom composition and flux at 20 keV to 500 keV with field of view of 90° × 107°, angular resolution of 8°, and energy resolution of 80%
EUV	Bill R. Sandel University of Arizona	Image plasmasphere.	Extreme ultraviolet irradiance at 30.4 nm with field of view of 90° × 90° and angular resolution of 0.6°
FUV	Stephen B. Mende University of California, Berkeley	Image electron and proton aurora; map geocorona.	Far ultraviolet irradiance at 135.6 nm, 121.8 nm, and 140–190 nm with field of view of 15° and angular resolution of 0.1°; geocorona maps with three 1° field-of-view photometers
RPI	Bodo W. Reinisch University of Massachusetts, Lowell	Sound total plasma density gradients throughout inner magnetosphere.	Sound total plasma density gradients throughout inner magnetosphere. Transmit and receive radio waves with frequencies between 3 kHz and 3 Mhz.

radiation; and radio sounding, which remotely determines total electron density. Table I also illustrates the measurement capabilities of each instrument. After two years of operation, each instrument continued to perform well and to contribute to the science objectives in a significant way.

Specific scientific achievements of the IMAGE mission during its first two years of operation include:

1. Determination of the spatial extent and location of the polar cusp as functions of the interplanetary magnetic field (Fuselier *et al.*, 2002a, 2003; Frey *et al.*, 2002).

2. Observation of prompt outflow of ionospheric ions following the arrival of a CME, indicating the existence of direct heating of the topside ionosphere (Fuselier *et al.*, 2001; Moore *et al.*, 2001).
3. Identification of global-scale ionospheric outflow as an immediate response to solar-wind pressure pulses (Fuselier *et al.*, 2002b, 2003);
4. Confirmation of the theory of plasmaspheric tails (Burch *et al.*, 2001a);
5. Discovery of several new and unpredicted features of the plasmasphere including "shoulders", "fingers", corotating "voids", and isolated flux tubes (Burch *et al.*, 2001b; Sandel *et al.*, 2001);
6. The use of solar wind data and the Magnetospheric Specification Model to relate the plasmasphere shoulders to south-north transitions in the interplanetary magnetic field (Goldstein *et al.*, 2002);
7. Discovery of subauroral proton arcs and identification of the role of the IMF in their formation (Immel *et al.*, 2002; Burch *et al.*, 2002);
8. Determination of the energy-dependent injection and drift of energetic ions during magnetospheric substorms (Burch *et al.*, 2001a;);
9. Acquisition of the first global images of the geomagnetic storm ring current, thereby identifying the development of a symmetric ring current during the recovery phase (Burch *et al.*, 2001a; Mitchell *et al.*, 2001; Pollock *et al.*, 2001).
10. Acquisition of global images of substorm dipolarization in the plasma sheet. (Brandt *et al.*, 2002);
11. Clarification of the relationships between substorms and magnetic storms, e.g., O^+ injection into ring current caused by substorms (Mitchell *et al.*, 2003);
12. Acquisition of the first global images of the proton aurora, establishing its cause and effect with correlative measurements of proton precipitation on FAST, and determination of the dynamical relationship between electron and proton aurora during substorms (Frey *et al.*, 2001; Mende *et al.*, 2001);
13. The first remote measurements of plasmaspheric densities using radio sounding (Reinisch *et al.*, 2001);
14. Identification of plasmaspheric cavities as source regions for kilometric continuum radiation (Green *et al.*, 2002);
15. The first measurements of solar-wind neutral atoms and interstellar neutral atoms from inside the magnetosphere. (Moore *et al.*, 2001, 2003; Collier *et al.*, 2001).

The early results from IMAGE represent significant progress toward answering the mission's scientific objectives. All of the instruments have contributed significantly to the scientific achievements of IMAGE in no small part because of the integrated nature of the payload and the resulting data stream, which uses a common format that facilitates the joint plotting of data. IMAGE has also contributed to the NOAA space forecasting activity through the ancillary real-time transmission of the entire IMAGE data set in addition to its baseline store-and-forward data mode.

While IMAGE is well on its way to achieving the full set of science objectives for the prime mission, an equally important extended mission will be possible because of the migration of the line of apsides of the IMAGE orbit toward lower latitudes (at a rate of 50 deg./yr.) and the transition to the declining phase of the solar cycle (during which CME-driven storms are generally replaced by recurring storms associated with high-speed streams at corotating interaction regions). The lower-latitude apogee will be especially useful for (1) the measurement of the distribution of energetic neutral atoms along magnetic flux tubes; (2) the measurement of global ionospheric outflow over both the northern and southern polar caps; (3) higher spatial resolution imaging of the aurora over both hemispheres; (4) radio sounding of the dayside magnetopause; (5) the measurement of plasmasphere refilling rates using EUV imaging of helium ions; and (6) radio sounding of the substorm-related changes in magnetic field line lengths where the IMAGE orbit is nearly field aligned.

The following sections review a subset of the major accomplishments of the IMAGE mission during its first two years of operation and provide a brief sketch of the new science objectives that will be made possible from the different orbital and solar conditions that will prevail during the extended mission.

2. Scientific Achievements of IMAGE

The scientific results of the IMAGE prime mission can be organized roughly along the lines of the three specific science objectives; which deal with plasma injection, both from the solar wind and from the ionosphere; the immediate, or directly driven, response of magnetospheric plasmas to changes in the solar wind and its magnetic field; and the transport, energization and loss of magnetospheric plasma. The discussion is illustrative rather than complete because the shear volume of new results could not be covered in the space allowed. However, much more detail is contained in the other papers of this special issue.

2.1. Plasma Injection

2.1.1. *Solar Wind Plasma Injection*

Solar wind plasma is heated and slowed by the Earth's bow shock, allowing it to flow around the magnetosphere in the magnetosheath. A small fraction of the magnetosheath plasma is injected directly into the magnetosphere and down to the dayside ionosphere through the polar cusps. Based on the movement of cusp particle precipitation in response to changes in the interplanetary magnetic field direction and on the proton velocity dispersion that is observed in the cusp, it has been generally believed that cusp injection results mainly from reconnection between geomagnetic and interplanetary magnetic fields. However, until now there has been no way to image the cusp, which is needed to confirm other predictions of

the magnetic reconnection model. Imaging of doppler-shifted Lyman-alpha emissions of precipitating energetic hydrogen atoms provides a unique global view of the proton aurora, as described by Mende (2000) and Fuselier *et al.* (2002a). On the dayside of the Earth, this view includes images of the ionospheric footprint of the cusp, which map the spatial extent and location of the cusp under varying solar-wind conditions with a time resolution of two minutes.

Figure 1 shows a global image of the proton aurora during a period of high solar-wind dynamic pressure (see Figure 2). As described by Fuselier *et al.* (2002a, 2002b), since the FUV SI-12 instrument images photons emitted by neutral hydrogen atoms with a kinetic energy component along the field of view of ∼4 keV, while solar-wind energies are typically ∼1 keV, either high solar-wind densities or high velocities are needed to produce significant responses from the instrument. In Figure 1, the footprint of the cusp is observed as a "spot" located in the pre-noon sector poleward of an incompletely developed main oval. The emission feature equatorward of the nominal oval (the q aurora) maps to near geosynchronous orbit and is produced by protons precipitating from the ring current (see Section 2.2.2). The cusp footprint is located where it would be expected to be observed for the case of high-latitude reconnection under conditions of positive B_z and negative B_y (Milan *et al.*, 2000). The Geotail data shown in Figure 1 establishes that the IMF at this time had indeed been strongly northward, with a significant negative B_y component, for the previous 40 minutes. Fuselier *et al.* (2002a) used the Tsyganenko model to confirm that the observed cusp emission for a similar event on June 8, 2000 occurred on field lines that mapped to the high-latitude pre-noon magnetopause, that is, to a region where, under the given solar wind conditions, the lobe field lines and magnetosheath field lines were oppositely oriented and thus antiparallel merging would be expected to occur. This event and several similar events that the IMAGE team has analyzed have confirmed predictions and previous in situ observations concerning the occurrence of high-latitude reconnection during northward IMF and corroborated observations showing the dependence of the location of the cusp footprint in local time on B_y (Newell *et al.*, 1989; Milan *et al.*, 2000). Further, the mapping of the cusp footpoint has provided information about the morphology of the high-latitude merging region, indicating that it is a narrow strip that extends tailward and comprises only a few percent of the total surface area of the magnetopause (Fuselier *et al.*, 2002a). The results of this analysis have important implications for our understanding of merging and plasma entry under varying IMF conditions.

For southward IMF conditions, the cusp migrates southward, merging with the proton auroral oval, and spreading out significantly in local time (Fuselier *et al.*, 2002a). By measuring the local-time extent of the cusp and tracing cusp field lines outward to the dayside magnetopause, it is possible to estimate the magnetopause reconnection rate. In addition, by tracing the locus of the cusp for various IMF directions, Fuselier *et al.* (2003) have been able to apply critical tests to the antiparallel and component merging hypotheses.

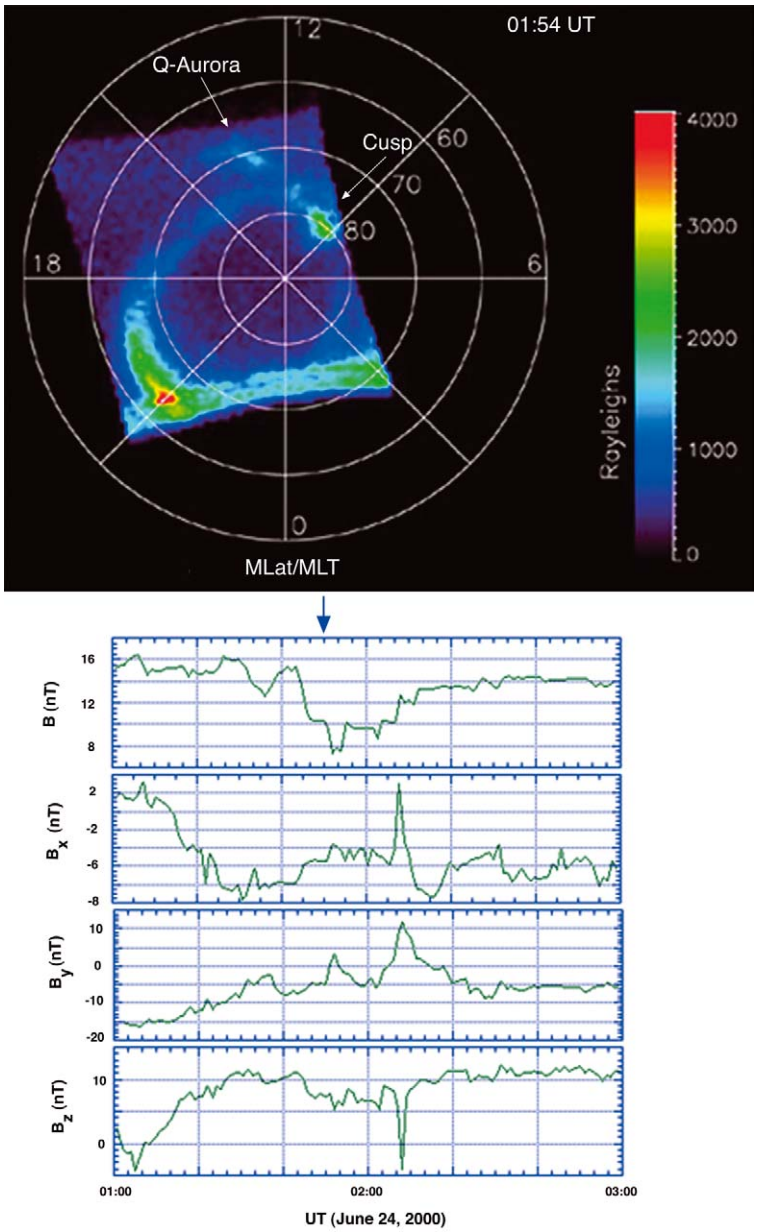

Figure 1. FUV SI-12 image of the proton aurora and Geotail interplanetary magnetic field data in GSE coordinates for northward IMF conditions on June 24, 2000. Geotail was located just outside the bowshock, and the calculated delay time between Geotail and the Earth is four minutes. This delay is taken into account by the arrow noting the time of the proton aurora image (Fuselier *et al.*, 2001b).

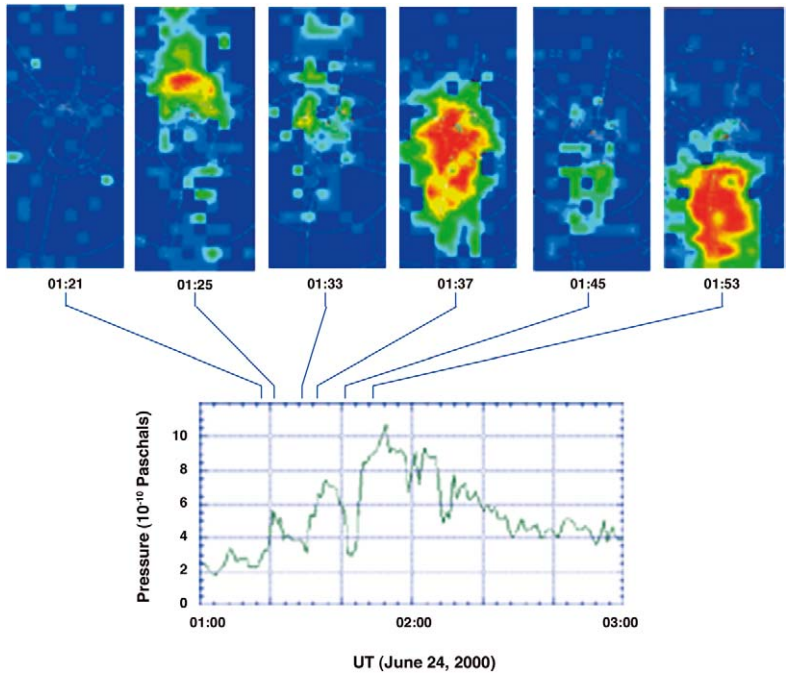

Figure 2. LENA images of ionospheric neutral-atom outflow (top) along with Geotail solar-wind pressure data (bottom on June 24, 2000). The time delay between Geotail and the Earth was four minutes, and this delay is taken into account in the time markers associating the LENA images with the Geotail data (Fuselier *et al.*, 2002).

2.1.2. *Ionospheric Outflow*

During magnetic storms, injections of heavy-ion (O^+) plasma from the high-latitude ionosphere are known to be an important source of magnetospheric plasma. In fact, ring current enhancement and decay are determined in large part by the motions of terrestrial O^+ ions during the largest storms (Hamilton *et al.*, 1988). Much in-situ evidence has been obtained that the largest mass flux of ionospheric plasma comes from the dayside auroral regions, and that it feeds into the nightside plasma sheet through the tail lobes. However, this plasma travels slowly, and it was not clear that it could arrive at the nightside acceleration regions soon enough to be a factor in storm development.

Correlative analysis of IMAGE FUV observations of dayside auroral emissions and LENA observations of polar ion outflow has made it possible to investigate the timing between the impulsive input of energy into the ionosphere and the resulting ionospheric outflow. Images of the Earth's proton aurora from FUV SI12 indicate a temporally and spatially isolated brightening of the proton aurora in the post-noon sector in immediate response to a CME-driven shock that impinged on the Earth's magnetopause at 0912 UT on June 8, 2000 (Fuselier *et al.*, 2001). A little over half an hour after the observed brightening, LENA detected a sharp

increase in ionospheric plasma outflow. The time delay between the auroral response and the enhanced outflow is consistent with the travel time of ∼30 eV neutral oxygen (created by charge exchange of outflowing O^+ with the exosphere) from the ionosphere to the spacecraft. This result indicates that the outflow was initiated immediately after the deposition of auroral energy as a result of the shock-induced magnetospheric disturbance. The promptness of the outflow indicates that energy sufficient to initiate the outflow was deposited near or above the O^+ exobase (∼350–1000 km) rather than at lower altitudes (e.g., around 250 km, where the bulk of the frictional ion heating occurs). This result localizes the ionospheric outflow to the dayside subsolar region and constrains the initial acceleration region to be well above 250 km altitude.

Fuselier *et al.* (2002b) provided further evidence of the prompt outflow of ionospheric plasma with an event on June 24, 2000 in which three successive solar wind pressure pulses impacted the magnetosphere. All three pressure pulses were associated with solar-wind density increases rather than velocity increases. The event, which spans the same time period as Figure 1, is shown in Figure 2. The alternating upper panels of Figure 2 show clear enhancements of ionospheric outflow in concert with the solar-wind pressure pulses measured by Geotail. Also seen in Figure 2, is a progression of the ionospheric outflow from the morning side toward the evening side. As explained by Fuselier (2003), this movement is caused primarily by the changing imaging perspective as the IMAGE spacecraft climbs from perigee toward apogee and from the night side toward the day side. The range of neutral-atom pitch angles that can be viewed by the LENA instrument depend upon the spacecraft position and the altitude at which the outflowing ions are neutralized by charge exchange. As shown by Fuselier (2003), the outflowing ions in the final LENA image panel of Figure 2 are associated with the bright auroral feature that is located near 21 MLT in Figure 1.

2.2. Directly Driven Response to Solar Wind Variations

2.2.1. *Plasmaspheric Tails and Shoulders*

A long-standing controversy has existed about the theoretical predictions of long plasma tails in the dusk hemisphere during magnetic storms. Spacecraft in geosynchronous orbit, as well as elliptically-orbiting spacecraft such as OGO-5, have for many years observed outlying enhancements of plasma density that could be interpreted as islands of plasma or as plasma tails. There was no way to resolve this controversy without global imaging, and one of the first scientific results of IMAGE was to resolve it in favor of the plasma tails (Burch *et al.*, 2001a; Sandel *et al.*, 2001). Figure 3 shows a false color image of a plasma tail event on August 11, 2000 with the Earth placed in position for reference.

In addition to the plasma tails, IMAGE has also observed other longitudinal gradients in the plasmapause such as “shoulders,” “fingers,” “voids,” and isolated flux tubes. While the theory of Grebowsky (1970) adequately accounts for the

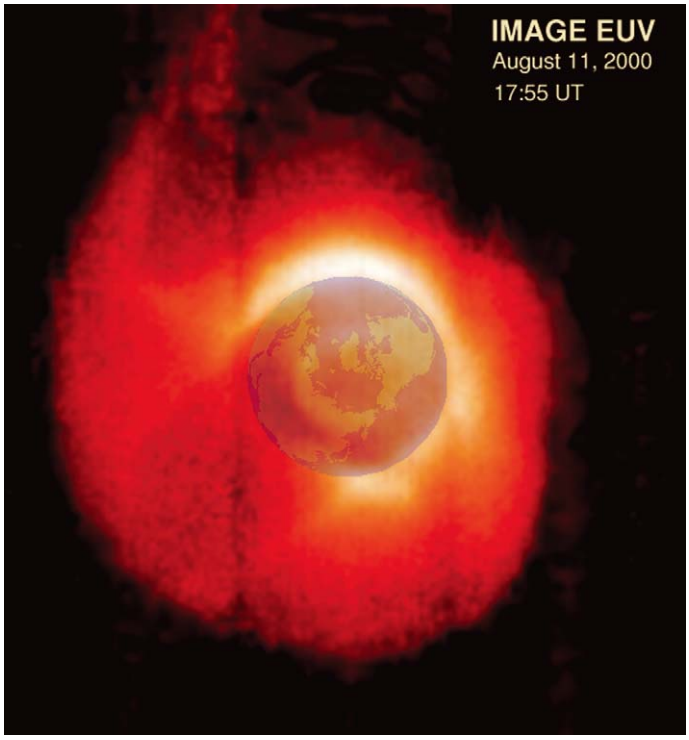

Figure 3. EUV image of the plasmasphere on August 11, 2000. The Sun is toward the upper right, opposite the midnight shadow region. A plasma tail is seen extending into the dusk-side and afternoon quadrants. The Earth has been added for reference.

development of plasma tails during the enhanced convection of magnetic storms, the other features had not been predicted and require explanation. The four images in the upper part of Figure 4 show an example of a plasmasphere with both a tail and a shoulder, which corotates with the Earth. Using the Rice University Magnetospheric Specification Model, Goldstein *et al.* (2002) have demonstrated that the development of the shoulder is a result of residual shielding of the convection electric field, which causes a reverse eddy of convection in the dawn sector when the IMF rotates from southward to northward. The south-north transition occurred at about 04:30 UT on May 24, 2000, as seen in the Geotail data of Figure 4. At that time, the IMAGE spacecraft was too close to perigee to allow plasmasphere images to be obtained. However, the MSM, which is an empirical model using actual solar wind data as input, shows clearly in this and other cases the development of a shoulder in the early morning hours in direct response to south-north IMF transitions.

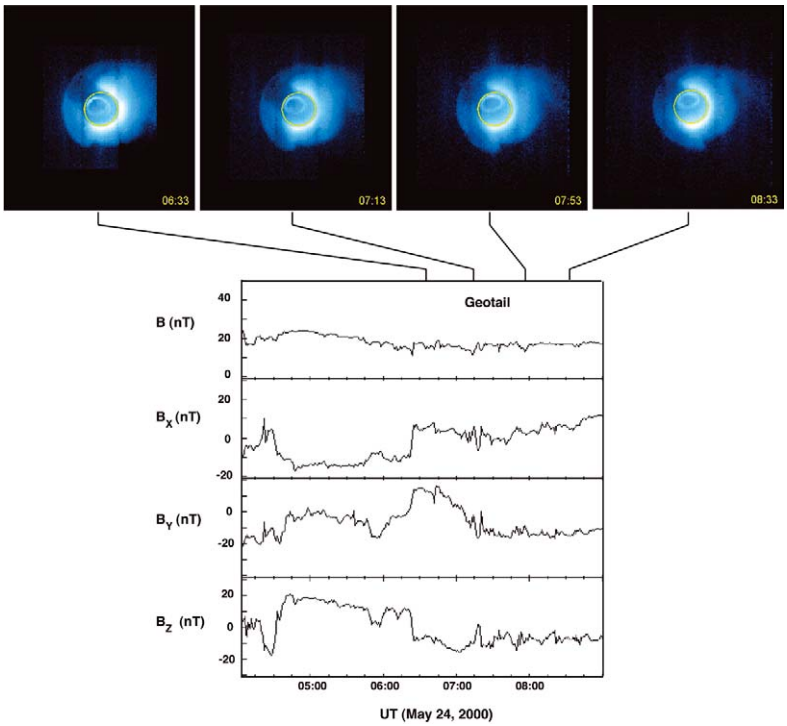

Figure 4. EUV images of the plasmasphere and Geotail IMF data on May 24, 2000. In each plasmasphere image the Sun is toward the lower right, opposite the midnight shadow region. The Earth's limb is noted by a yellow circle. A plasma tail is seen in the upper right-hand part of each image, while a plasmaspheric shoulder can be seen corotating with the Earth in the lower part of each image. Also visible in each image is the EUV aurora.

2.2.2. *The Q-Aurora*

Immel *et al.* (2002) and Fuselier *et al.* (2002b) used FUV SI-12 proton aurora images to discover subauroral proton arcs in the afternoon sector of the northern hemisphere during periods of high solar-wind pressure. The proton precipitation was confirmed by Immel *et al.* with FAST particle data in the magnetically conjugate region in the southern hemisphere. Later, Burch *et al.* (2002) identified south-north and west-east IMF rotations as causes of the arcs' appearance. In addition, Burch *et al.* provided further confirmation of the proton precipitation into the arcs with northern-hemisphere DMSP data and noted a possible connection to plasmaspheric tails using data from LANL geosynchronous satellites.

Figure 5 shows proton aurora images before and after the formation of the subauroral proton arc in an event studied by Burch *et al.* (2002). Because of the overall appearance of the main proton oval and the appended subauroral arc, these arcs are often referred to as q-auroras. The auroral image on the left-hand side of Figure 5 does not show the q-aurora, even though a very active proton oval is apparent during this period of moderate to intense substorm activity (Burch

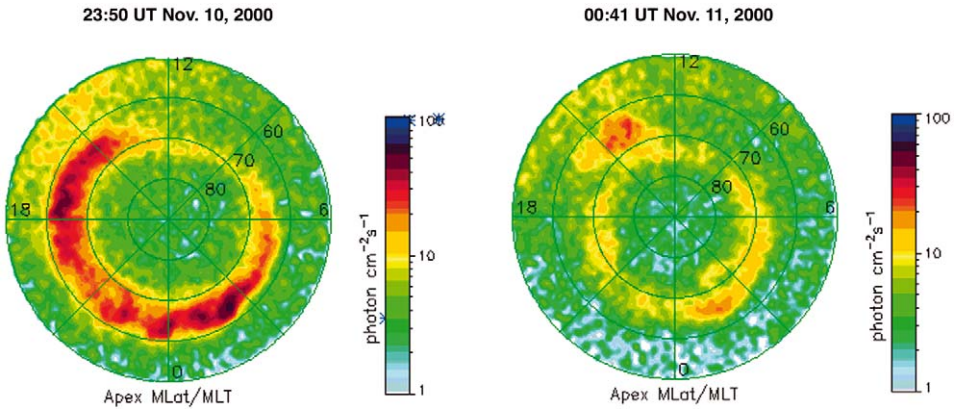

Figure 5. FUV SI-12 proton aurora images at 23:50 UT on November 9, 2000 (left image) and 00:41 UT on November 10, 2000. The IMF had a southward component at the time of the left-hand image and a northward component at the time of the right-hand image, as shown by Burch *et al.* (2002).

et al., 2002). The IMF had a southward component at this time. Fifty-one minutes later, the image on the right-hand side of Figure 5 shows that the proton oval had shrunk dramatically toward the invariant pole as the IMF turned northward. However, the proton auroral emissions in the afternoon sector did not move poleward but stayed at approximately the same latitude, forming the q-aurora. Burch *et al.* (2002) also showed another event in January 2001 during which a q-aurora formed following a rotation of the IMF Y component from negative to positive. In this case, the afternoon-quadrant oval was shifted toward the dawn side as predicted in the models of Burch *et al.* (1985) and Cowley *et al.* (1991), again leaving the subauroral arc at the original oval location in the afternoon sector. This result is the first confirmation of these long-standing model predictions.

2.3. Transport, Energization, and Loss of Plasma

2.3.1. *Substorm and Magnetic Storm Plasma Injection and Drift*

The IMAGE mission has determined fundamental differences between storms and substorms with regard to the injection of energetic particles into the inner magnetosphere. In the case of substorms, the plasma-sheet ion injection at energies above 10 keV rarely penetrates deeper than 6 or 7 R_E in the nightside equatorial magnetosphere (Mitchell *et al.*, 2001; Pollock *et al.*, 2001). The energetic ions then drift by the well-known curvature and gradient drift mechanisms, before leaving the magnetosphere through the magnetopause along the dusk flank and the dayside. The lower-energy ions (less than around 10 keV) do not undergo drift dominated by magnetic gradient and curvature. Rather, they appear to stagnate on the night side. At even lower energies, the transport of injected ions may be dominated by convection, with ions drifting toward the day side via either dusk or dawn.

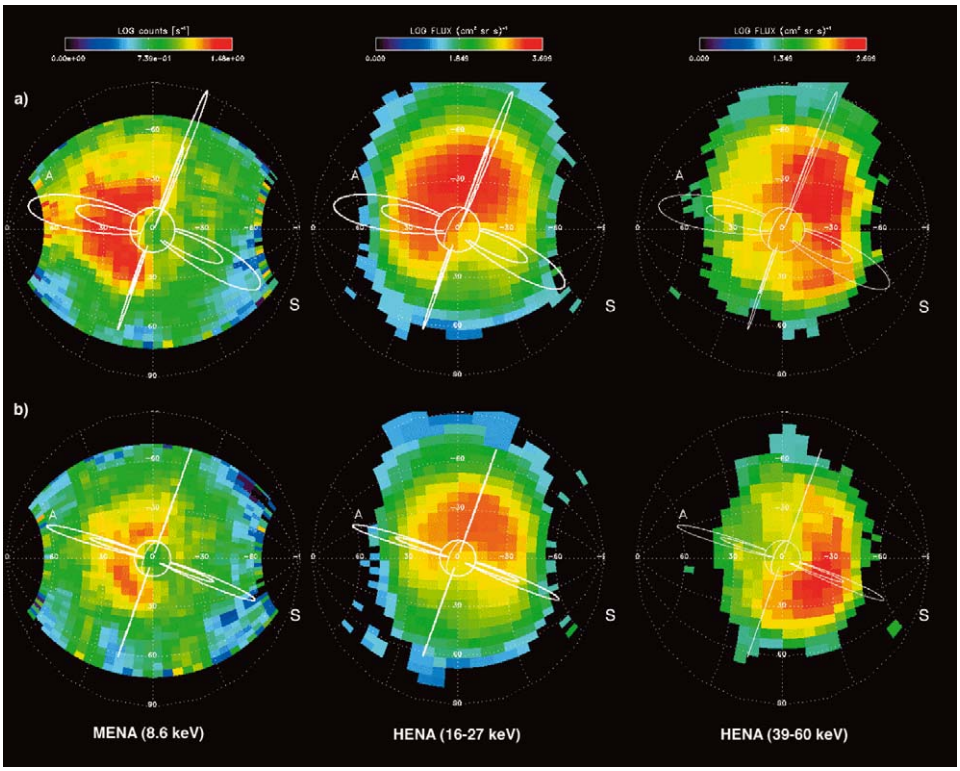

Figure 6. ENA images at three different energies during a substorm on June 10, 2000. Images in the top row were obtained at 11:00 UT, during the peak of substorm activity; those in the bottom row were taken during substorm recovery at 11:40 UT. The Earth is shown as a white circle in the middle of each image. Dipole magnetic field lines are shown for L = 4 and 8; the S and A denote the sunward and antisunward field lines.

Figure 6 illustrates this ENA evolution observed by MENA and HENA during the late expansion phase of a substorm on June 10, 2000 (images A, B, C, at 1100 UT) and well into the recovery phase (images D, E, F, at 1140 UT) (Burch *et al.*, 2001a). In the top row, strong injection is seen at 8.6 keV on the nightside, while higher-energy ions have drifted well past the dusk meridian. Forty minutes later, the lower energy end of the ring current injection has diminished in intensity while the higher-energy ions have drifted around the dusk and dayside hemispheres and finally to the dawn meridian. The substorms on June 10, 2000 occurred during the extended recovery phase of a magnetic storm as shown by the DsT plot in Figure 7 (yellow arrow).

For large magnetic storms, the ions in the 10 to 100 keV energy range penetrate much closer to Earth during the main phase injection, where they drift on closed drift paths, forming a symmetric ring current (Burch *et al.*, 2001a). Figure 7 shows an example of a fully developed symmetric ring current during the earlier recovery phase of the same magnetic storm on June 9, 2000. Storm-time behavior differs

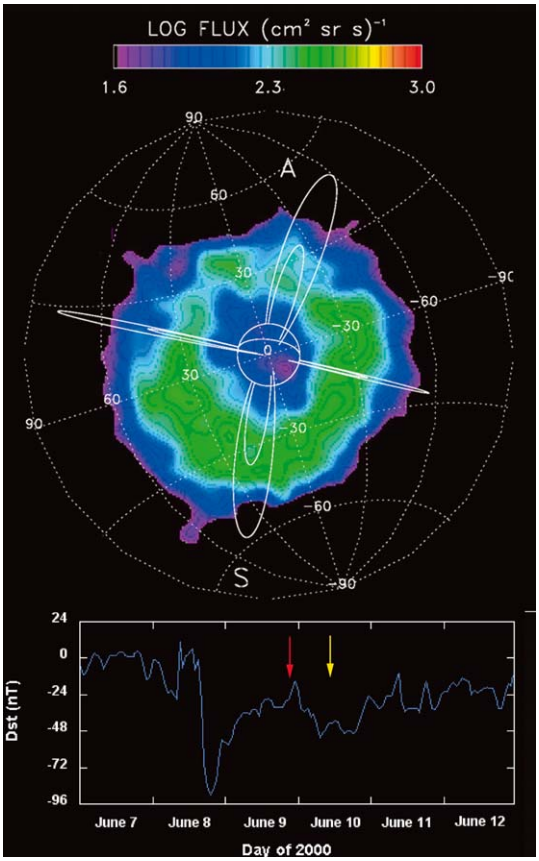

Figure 7. HENA ENA image of a symmetric ring current during the recovery phase of a magnetic storm at 21:18 UT on June 9, 2000. As in Figure 6, the Earth is shown as a white circle; L = 4 and L = 8 dipole magnetic field lines are shown as white lines, and S and A denote the sunward and antisunward directions, respectively. The time of the image is noted by the red arrow in the Dst plot in the bottom panel of the figure. The yellow arrow notes the time of the first set of images in Figure 6.

from the substorm case, where the energetic ions remain concentrated on the night and dusk sides, until they are lost from the magnetosphere after one to a few hours. In large storms, once the ions become trapped, they drift for days on their closed, nearly circular drift paths, gradually diminishing in numbers as they are lost by charge-exchange, coulomb collisions, and wave-particle interactions.

2.3.2. *Substorm Magnetic Field Dipolarization*

Measurements of the magnetic field in the near-Earth magnetotail (∼8–10 R_E), and inward to geosynchronous orbit, have for many years shown evidence for a "dipolarization" of the field at substorm onset (McPherron *et al.*, 1973). The magnetic field in this region undergoes a "stretching" to a more tail-like topology

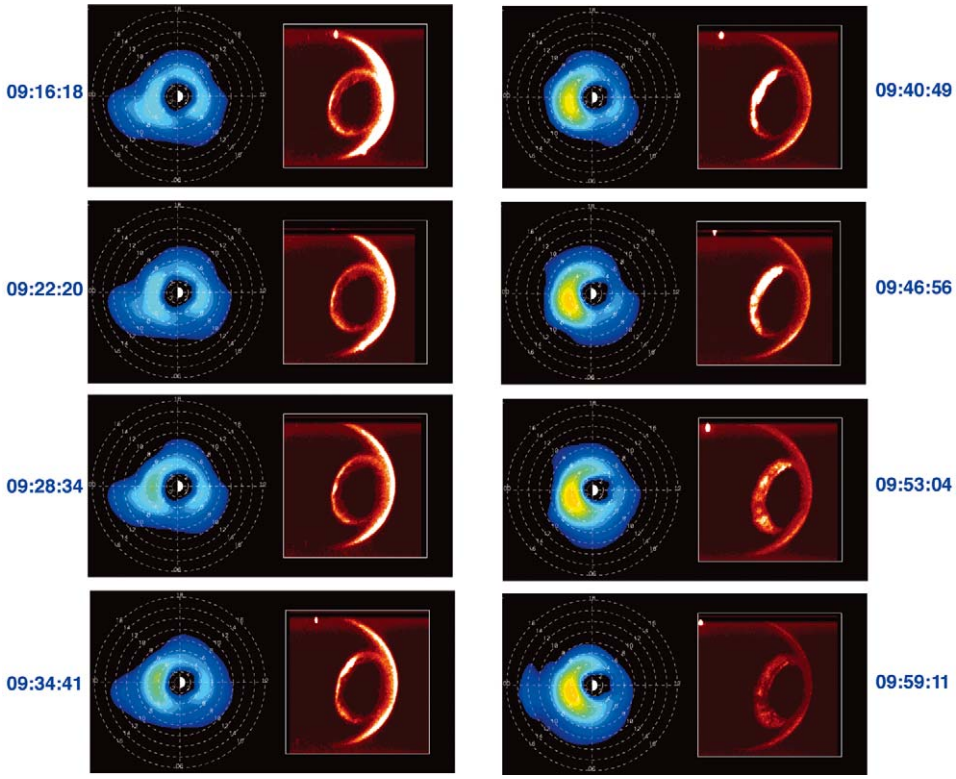

Figure 8. HENA equatorial ion images at 27–60 keV (deconvolved from ENA images) at 6-minute intervals on October 4, 2000 shown alongside FUV-WIC broadband UV auroral images. The Sun is to the right in each image. The circular grids on the ion images are drawn at two-R_E intervals out to 16 R_E. The ion fluxes are presented in a logarithmic color scale, while the auroral images are presented in a linear Rayleigh scale. A dipole magnetic field is assumed (see Brandt *et al.*, 2002b).

as a result of enhanced neutral sheet current densities and Earthward motion of the neutral-sheet current during the growth phase of substorms. At substorm onset, a process described as neutral-sheet diversion (McPherron *et al.*, 1973) or neutral-sheet disruption (Lui *et al.*, 1990) causes the stretched growth-phase field to return to a more dipole-like configuration. Although this dipolarization is an accepted feature of substorms, with HENA ENA images it has been imaged for the first time, as reported by Brandt *et al.* (2002). Figure 8 shows HENA ion images (deconvolved from the ENA images) and FUV WIC broadband UV auroral images for the substorm event on October 4, 2000 that was reported by Brandt *et al.* (2002).

Figure 8 displays only every third image obtained by HENA and FUV WIC during the October 4, 2000 substorm. Nonetheless, even with six-minute time resolution the onset, expansion, and recovery of the substorm are clearly seen within the 50-minute time period covered by Figure 8. Most striking are the changes in the ion images that occur in concert with the intensification, spreading, and subsequent weakening of the global auroral displays. The rapid Earthward motion of

the plasma sheet ions, as is expected to occur with dipolarization is clearly seen between 09:34:41 UT and 09:40:49 UT with the outer boundary of the plasma sheet near midnight moving rapidly inward from near 13 R_E to near 8 R_E and back again. These distances agree with the region of observed dipolarization in the magnetic tail.

2.3.3. *Oxygen Injection into the Ring Current During Substorms*

The ability of the HENA instrument to obtain separate ENA images for hydrogen and oxygen has led to the discovery of a significant aspect of the role of substorms in the development of magnetic storms (Mitchell *et al.*, 2003). The result is illustrated in Figure 9, the top panel of which shows FUV SI-12 images of the proton aurora. The second panel shows the corresponding H (27–60 keV) and O (98–264 keV) ENA images once every 30 minutes between 12:00 UT and 14:00 UT on October 1, 2001. The third panel of Figure 9 shows daily spin-phase versus time spectrograms for H (39–50 keV) and O (180–222 keV). The dark regions between 07 and 10 UT and between 22 and 24 UT result from passage of the spacecraft through the radiation belts (where the HENA detectors are turned off to protect from high counts from penetrating radiation). A brief period of imaging at perigee can be seen near the center of each dark region. The bottom two panels show provisional AE and Dst values, respectively.

Each vertical line in the spectrograms represents an image like those in the second panel but with the polar angles of each image summed together at each spin angle. The 0° spin angle is the position of the center of the Earth. As the spacecraft nears perigee, it is clear that the ENA fluxes fill more of the field of view of HENA as the radial distance of the equatorial intersection of its field of view gets much smaller. Comparison of the many images collapsed into the two spectrograms with the AE and Dst traces shows clearly that the intensities of the hydrogen images vary smoothly in accordance with the growth and decay of Dst, while the oxygen ENA images are much more impulsive and follow generally the substorm intensifications shown by the AE trace. This correspondence is especially striking for the substorm with peak intensity near 12:30 UT.

Mitchell *et al.* (2003) have noted that the substorm-associated intensifications of ring-current O^+ occur only during magnetic storms and not for isolated substorms. The prominence of O^+ injections as compared to H^+ can be explained by induced electric fields produced by magnetic-field dipolarization (Delcourt, 2002). As shown by Delcourt, O^+ ions originating from the ionosphere during previous substorms undergo non-adiabatic acceleration up to hundreds of keV while being injected earthward. H^+ ions, on the other hand, have shorter gyro periods, which may allow them to follow the dipolarization more adiabatically and hence experience much less acceleration.

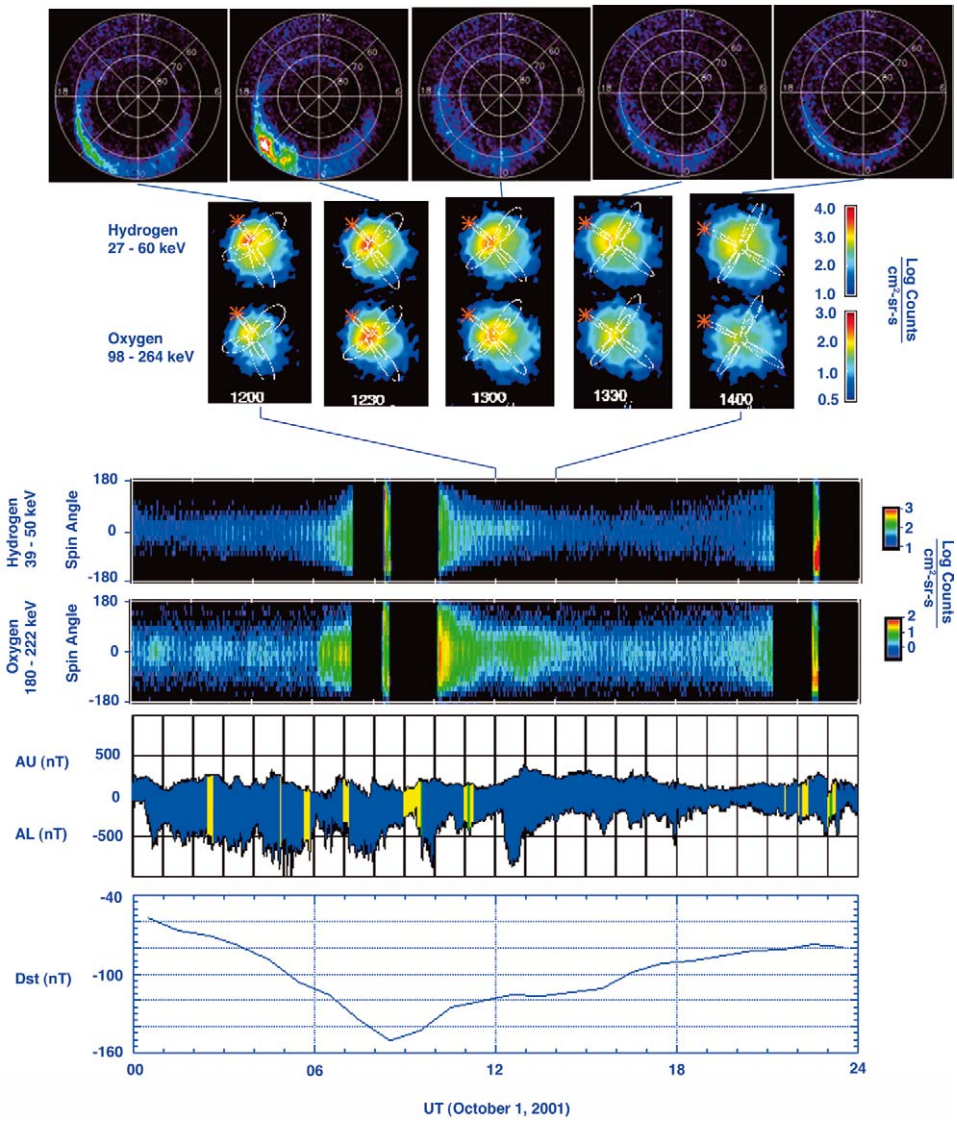

Figure 9. FUV SI-12 proton aurora images (in Λ-MLT format with noon at the top) at 30-minute intervals from 12:00 to 14:00 UT on October 1, 2001 (top panel). Hydrogen and oxygen ENA images for the times corresponding to the SI-12 images in the same format as Figures 6–7 except the noon field lines are marked with a red asterisk (second panel). Hydrogen and oxygen ENA spin-angle vs. time spectrograms for the full day (third panel). AE and Dst indices (bottom two panels).

2.3.4. *Substorm Dynamics of Electron and Proton Aurora*
FUV data presented by Mende *et al.* (2002) show the development, during the expansive phase of a substorm, of a double oval configuration, consisting of a set of discrete poleward forms and a separate equatorward diffuse auroral oval. A simultaneous FAST pass provided a diagnostic of the particle types in the various regions. From these data, it was seen that in the late substorm expansive phase and recovery phase the auroral oval had five components in order of decreasing latitude: a) active (convecting) irregular forms inside the polar cap and near the polar cap/auroral oval boundary, b) a region of discrete auroras consisting mainly of arcs, c) a gap consisting of lower precipitation intensities, d) a region of diffuse auroras with occasional embedded structure, and e) a region of proton auroras slightly equatorward of and overlapping the diffuse aurora. Simultaneous plasma observations from FAST were consistent with the imaging data. The low-latitude region shows mainly diffuse precipitation. There is a gap, and poleward of the gap are high-intensity, electrostatically-accelerated electrons. Immediately poleward of these electrons, another group of electrons are seen with broader energy spectra characteristic of acceleration by wave-particle interactions. These results have built upon the double-oval descriptions of Elphinstone (1995a, b) by adding information on the morphology of the proton aurora and the acceleration characteristics of the auroral particles. In addition, Mende *et al.* (2002) have shown that the double-oval configuration persists into the substorm recovery phase and that the Alfvén-accelerated electrons are associated with either short-lived or rapidly-moving auroral features.

2.3.5. *Plasmasphere Refilling and Ducts*
The outer plasmasphere has been sampled by previous spacecraft but never before probed remotely from space. RPI radio soundings show large regions within and beyond the plasmasphere to be permeated by field-aligned irregularities or ducts, which strongly influence high-frequency wave propagation. These ducts make possible the study of an important class of magnetosphere-ionosphere plasma interchange processes. It has been found that the RPI waves can propagate efficiently to great distances along field lines within these plasma ducts extending down into the northern polar region and into the conjugate hemisphere near and within the plasmasphere. The ducts are slight density depletions, estimated to be down about 10% from their surrounding field lines.

The left-hand panel of Figure 10 (from Carpenter *et al.*, 2002) is an RPI plasmagram (Reinisch *et al.*, 2001) – the magnetospheric analog of an ionogram. A plasmagram is a plot of echo amplitude (color scale) as a function of frequency and echo delay. Both ducted (field-aligned) and direct echoes from the plasmasphere are labeled in the Figure 10 plasmagram. The ducted echoes can be inverted to reveal the field-aligned density structure of the plasmaspheric filling regions. The density profiles obtained from this type of analysis often deviate significantly from diffusive equilibrium and show plasma accumulation along the field line at high

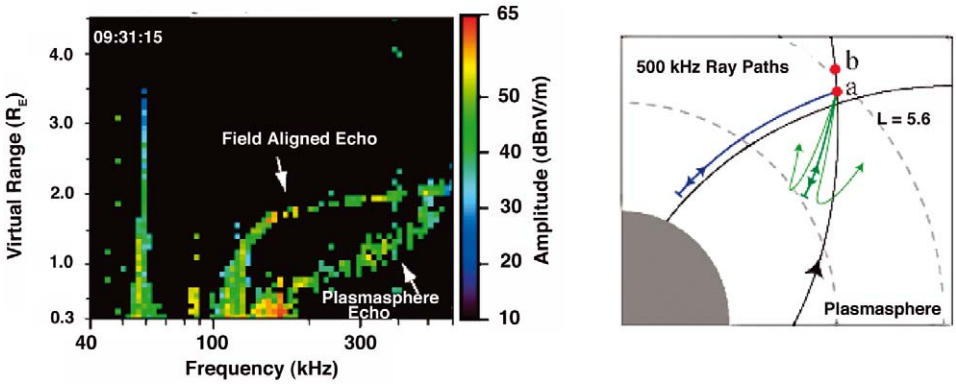

Figure 10. RPI plasmasphere sounding. Left panel shows a frequency-time spectrogram (with time converted to distance to the reflection point). Right panel shows a schematic of ducted and direct-echo sounding of the plasmasphere. The IMAGE orbit and direction is shown in the right panel (Carpenter *et al.*, 2002).

altitude. Such observations might suggest top-down plasmaspheric filling (Singh and Horwitz, 1992). However, even that model does not accommodate the observed deviation from diffusive equilibrium and more detailed analysis of plasmaspheric ducted echoes is clearly needed (Green and Reinisch, 2003).

2.3.6. *Kilometric Continuum Radiation*

The Radio Plasma Imager (RPI) and the Extreme Ultraviolet (EUV) Imager instruments are providing new observations of the source region of kilometric continuum (Green *et al.*, 2002). The IMAGE observations show that kilometric continuum is generated at the plasmapause, from sources in or very near the magnetic equator, within a bite-out region of the plasmasphere. It is not known if the bite-out region is a necessary condition for the generation of kilometric continuum. From ray tracing calculations in a model plasmasphere having a bite-out feature, it is found that a kilometric continuum source can produce a relatively narrow emission cone that is largely confined to the longitudinal extent of the bite-out structure. Since the bite-out structure is observed to co-rotate with the plasmasphere, so would the beamed kilometric continuum. In addition, the observed narrow latitudinal extent of the emission cone does not appear to be a propagation effect but is perhaps produced by the emission mechanism, such as the linear or nonlinear mode-conversion processes at the upper hybrid resonance proposed by a number of investigators (e.g., Strangeway, 1985). The processes by which bite-out structures are produced in the plasmasphere are not completely understood at this time.

2.4. Heliospheric and Interstellar Neutral Atoms

One of the original ancillary science goals of the IMAGE mission was to search for solar-wind and interstellar neutral atoms, neither of which has ever been directly

observed in the inner solar system (although interstellar He was observed from the Ulysses spacecraft). With the LENA instrument, IMAGE has succeeded in detecting both neutral populations.

2.4.1. *Solar Wind Neutral Atoms*

Because of its excellent UV rejection, the LENA imager can detect neutral atoms coming from the solar direction (Moore *et al.*, 2001, 2003; Collier *et al.*, 2001). These neutral atoms are created by the exchange of charge between solar wind protons and the Earth's exospheric hydrogen. The charge exchange is thought to occur just outside the magnetopause in the magnetosheath (Moore *et al.*, 2001). The imager sees a weak, diffuse peak when the Sun is outside of its field of view and a sharp, intense peak when the Sun is within its field of view. The two different responses are the result of a difference in the Mach number of magnetosheath plasma compared to that of the upstream solar wind. Because the fast solar wind neutrals are not affected by the Earth's magnetic field, they provide a potential means of monitoring solar wind intensity from a vantage point inside the magnetosphere.

Solar wind neutrals are also created by charge exchange between the solar wind and interstellar neutrals. LENA data have revealed that the solar wind neutrals had a pronounced long-term variation over the first nine months of the mission (Moore *et al.*, 2003). This variation represents an azimuthal variation of the integral neutral gas density between the Sun and Earth and is loosely aligned with the known direction of motion of the solar system through the galaxy (Moore *et al.*, 2003). These observations of seasonal variations in the neutral solar wind component appear to be related to charge exchange of the solar wind with interstellar neutrals, which creates fast solar wind neutrals and interstellar ions. Analysis of these findings is still in progress but has the potential to yield information about the distribution of gas in the inner solar system.

2.4.2. *Interstellar Neutral Atom Sensing*

IMAGE has also directly observed the interstellar neutral atoms as the spacecraft was passing beyond the anti-apex direction downstream in the galactic gas flow (Moore *et al.*, 2003). The weak signal, which was predicted from a model involving solar gravitation and radiation pressure (S. Fuselier, private communication) to begin on 7 December 2000, actually appeared about 25 December 2000 and disappeared about 8 February 2001. The delay was due to masking by the solar wind neutral component. It was narrow in angular distribution and centered on the ram direction of the Earth's motion around the Sun. The appearance and disappearance of the direct interstellar neutrals in the LENA imager is closely associated with the field of view of the imager and the bending of interstellar neutral trajectories as they pass through the gravitational field of the Sun. Our study of this direct interstellar neutral signal, like that of the solar wind neutrals, is just beginning. However, the detection of these neutrals in the inner solar system holds promise for future studies of the interstellar medium from the near-Earth environment.

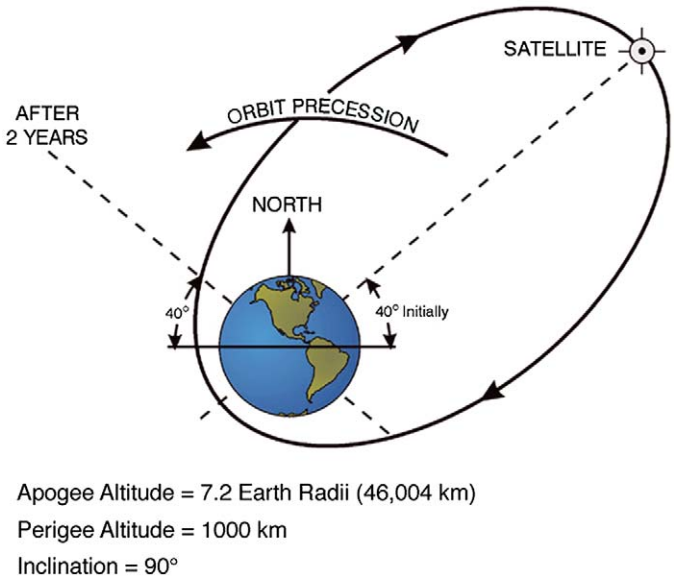

Figure 11. IMAGE orbit for the two-year prime mission. Local-time precession is not shown since the 90°-inclination orbit is fixed in inertial space. The initial apogee at launch on March 25, 2000 was at approximately 12:35 PM local time.

3. Image Extended Mission

The scientific accomplishments of IMAGE to date have opened the door to many new scientific discoveries. Beyond the prime mission, the progression through the solar cycle and the precession of the IMAGE orbit will provide the opportunity for an essentially new mission for IMAGE during the years 2002 through 2005. The focus of the new mission will be on the recurrent magnetic storms associated with high-speed solar wind streams and corotating interaction regions.

3.1. The Changing Imaging Perspective

During the two-year prime mission of IMAGE, the apogee, and hence the primary imaging perspective, remained above the northern polar cap (Figure 11). However, the relatively rapid precession of the 90-deg. inclination orbit will cause the imaging perspective to evolve through low latitudes and into the southern polar cap (Figure 12). While the high-latitude perspective provides full local-time imaging of magnetospheric plasmas, the ENA emissions from that perspective are often dominated by low-altitude sources because of higher exospheric densities. A mid to low-latitude imaging perspective, on the other hand, will complement the prime mission by allowing imaging of the distribution of the ENA emissions along magnetic flux tubes. An example from HENA on October 1, 2002, when apogee was at mid-latitudes, is shown in Figure 13. A similar consideration applies to EUV

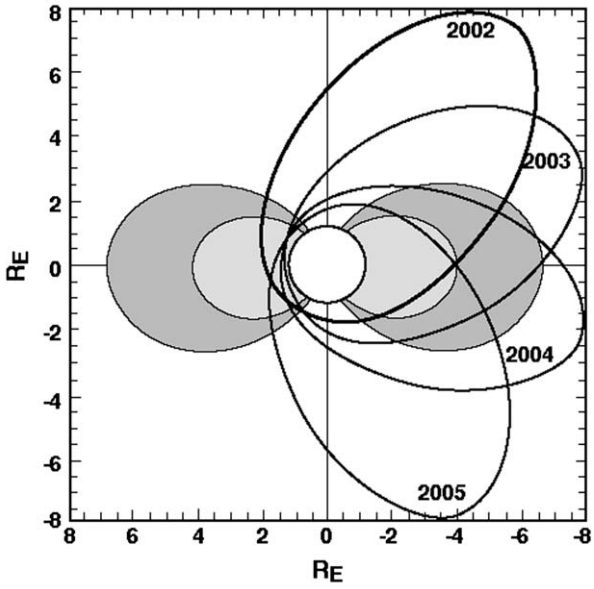

Figure 12. From March 2002 to March 2005, the IMAGE line of apsides will precess from high northern latitudes to high southern latitudes. Orbits are plotted in the orbit plane, in which right ascension = 12° (left half plane) and 192° (right half plane). The local-time precession is not shown since the 90°-inclination orbit is fixed in inertial space.

imaging of the plasmasphere. Other significant features of a lower-latitude apogee include the ability to image the aurora with FUV and the ionospheric outflow with LENA with higher spatial resolution and in both hemispheres in the ascending and descending parts of the orbit. Finally, with apogee at low latitudes on the day side, RPI will have its best opportunity to sound the magnetopause and track its motion. Moreover, during this phase of the mission a unique opportunity will exist for the RPI to make a variety of global observations while moving nearly along a constant L shell and observing field-aligned ducted echoes. This configuration will allow observations of plasmaspheric refilling and changes in magnetic field-line lengths during substorms.

3.2. Solar Cycle Effects

In addition to the changing imaging perspective, an epochal change in solar activity will be experienced during the extended mission. As time progresses from 2002 through 2005, magnetic activity will in general wane, but the mostly CME-driven storms of solar maximum will be replaced by the smaller, but possibly even more frequent, recurrent storms that typically occur during the declining phase of the solar cycle in association with coronal holes (Tsurutani *et al.*, 1995).

In addition to the changing character of magnetic disturbances, there are also well-known solar-cycle effects on the upper atmosphere. For example, IMAGE has

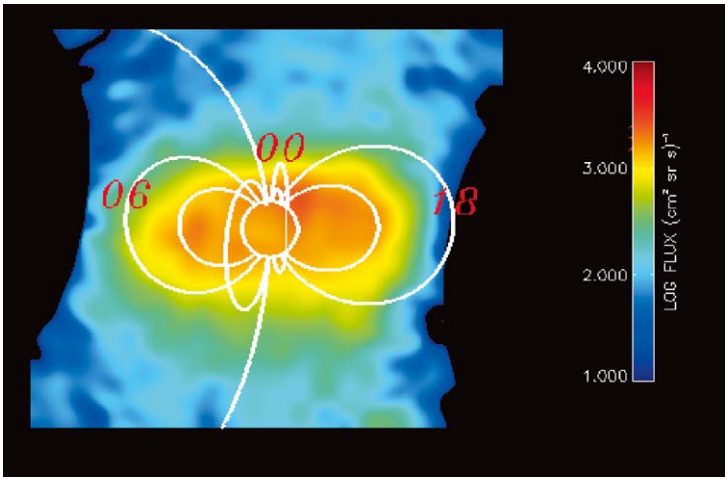

Figure 13. HENA 27–60 keV ENA image for the time period 09:09:58 to 09:19:58 UT on October 2, 2002, when the IMAGE apogee was at mid-latitudes.

shown that there is a prompt ionospheric outflow in response to input from the solar wind (Fuselier *et al.*, 2001). This prompt ionospheric outflow is the result of energy input into the topside ionosphere near the oxygen scale height. These observations were made during solar maximum when the exosphere is relatively hot and the oxygen scale height is high. In the declining phase of the solar cycle, the exosphere is expected to cool, the oxygen scale heights should drop, and the H density should increase. The net result of these effects may be an observable delay between the time of arrival of a solar wind feature that creates an ionospheric disturbance (such as a high-speed solar wind stream associated with a co-rotational interaction region) and the outflow observed by LENA. This delay could signal a change in the relative importance of various energization mechanisms. The lack of an observed delay would effectively eliminate certain acceleration mechanisms or at least severely reduce their importance.

Acknowledgements

The IMAGE program at Southwest Research Institute is supported by NASA Contract No. NAS5-96020. Principal investigators for the Geotail magnetometer and the two plasma instruments are Drs. S. Kokubun, L. A. Frank, and T. Mukai, respectively. Helpful discussions with Dr. W. S. Lewis are gratefully acknowledged. Provisional AE and Dst values are provided by the World Data Center C2 at Kyoto, Japan.

References

Brandt, P.C:Son *et al.*: 2002, 'IMAGE/HENA: Global ENA Imaging of the Plasma Sheet and Ring Current during Substorms', *J. Geophys. Res.* **107**, A12, 10.1029/2002JA009307.

Burch, J.L. *et al.*: 1985, 'IMF B_y-Dependent Plasma Flow and Birkeland Currents in the Dayside Magnetosphere, 1, Dynamics Explorer Observations', *J. Geophys. Res.* **90**, 1577–1594.

Burch, J.L.: 2000, 'IMAGE Mission Overview', *Space Sci. Rev.* **91**, 1–14.

Burch, J.L. *et al.*: 2001a, 'Views of Earth's Magnetosphere with the IMAGE Satellite', *Science* **291**, 619–624.

Burch, J.L. *et al.*: 2001b, 'Global Dynamics of the Plasmasphere and Ring Current During Magnetic Storms', *Geophys. Res. Lett.* **28**, 1159–1162.

Burch, J.L. *et al.*: 2002, 'Interplanetary Magnetic Field Control of Afternoon-Sector Detached Proton Auroral Arcs', *J. Geophys. Res.* **107**, A9,10.1029/2001JA007554.

Carpenter, D.L. *et al.*: 2002, 'Small-Scale Field-Aligned Plasmaspheric Density Structures Inferred From RPI on IMAGE', *J. Geophys. Res.* **107**, A9, 10.1029/JA009199.

Collier, M.R. *et al.*: 2001, 'Observations of Neutral Atoms from the Solar Wind', *J. Geophys. Res.* **106**, 24,893–24,906.

Cowley, S.W.H. *et al.*: 1991, 'Dependence of Convective Flows and Particle Precipitation in the High-Latitude Dayside Ionosphere on the *X* and *Y* Components of the Interplanetary Magnetic Field', *J. Geophys. Res.* **96**, 5557–5564.

Delcourt, D.C.: 2002, 'Particle Acceleration by Inductive Electric Fields in the Inner Magnetosphere', *J. Atm. Solar-Terr. Phys.* **64**, 551–559.

Elphinstone, R.D. *et al.*: 1995a, 'The Double Oval UV Auroral Distribution. 1. Implications for the Mapping of Auroral Arcs', *J. Geophys. Res.* **100**, 12,075–12,092.

Elphinstone, R.D. *et al.*: 1995b, 'The Double Oval UV Auroral Distribution. 2. The Most Poleward Arc system and the Dynamics of the Magnetotail', *J. Geophys. Res.* **100**, 12,093–12,102.

Frey, H.U. *et al.*: 2001, 'The Electron and Proton Aurora as Seen by IMAGE-FUV and FAST', *Geophys. Res. Lett.* **28**, 1135–1138.

Frey, H.U. *et al.*: 2002, 'Proton Aurora in the Cusp', *J. Geophys. Res.* **107**, 10.129/2001JA900161.

Fuselier, S.A. *et al.*: 2001, 'Ion Outflow Observed by IMAGE: Implications for Source Regions and Heating Mechanisms', *Geophys. Res. Lett.* **28**, 1163–1166.

Fuselier, S.A. *et al.*: 2002a, 'Cusp Aurora Dependence on Interplanetary Magnetic Field B_z', *J. Geophys. Res.* **107**, 10.1029/2001JA900165.

Fuselier, S.A. *et al.*: 2002b, 'Localized Ion Outflow in Response to a Solar Wind Pressure Pulse', *J. Geophys. Res.* **107**, 10.1029/2001JA000297.

Fuselier, S.A. *et al.*: 2003, 'Cusp Dynamics and Ionospheric Outflow, *Space Science Rev.*, this issue.

Goldstein, J. *et al.*: 2002, 'IMF-driven Overshielding Electric Field and the Origin of the Plasmaspheric Shoulder of May 24, 2000', *Geophys. Res. Lett.* **29**, 16, 10.1029/2001GL014534.

Grebowsky, J.M.: 1970, 'Model Study of Plasmapause Motion', *J. Geophys. Res.* **75**, 4329–4334.

Green, J.L., and B.W. Reinisch: 2003, 'An Overview of Results from the RPI on IMAGE', *Space Sci. Rev.*, this issue.

Green, J.L. *et al.*: 2002, 'On the Origin of Kilometric Continuum Radiation with Plasmaspheric Structures', *J. Geophys. Res.* **107**, 10.1029/2001JA000193.bur

Hamilton, D.C. *et al.*: 1988, 'Ring Current Development During the great Geomagnetic Storm of February 1986', *J. Geophys. Res.* **93**, 14,343–14,355.

Immel, T.J. *et al.*: 2002, 'Precipitation of Auroral Protons in Detached Arcs', *Geophys. Res. Lett.* **29**, 10.1029/2001GL013847.

Lui, A.T.Y. *et al.*: 1990, 'A Current Disruption Mechanism in the Neutral Sheet: A Possible Trigger for Substorm Expansions', *Geophys. Res. Lett.* **17**, 745–748.

McPherron, R.L. *et al.*: 1973, 'Satellite Studies of Magnetospheric Substorms on August 15, 1968 9. Phenomenological Model for Substorms', *J. Geophys. Res.* **78**, 3131–3149.

Mende, S.B. *et al.*: 2000, 'Far Ultraviolet Imaging from the IMAGE Spacecraft: 3. Spectral Imaging of Lyman-α', *Space Sci. Rev.* **91**, 287–318.

Mende, S.B. *et al.*: 2001, 'Global Observations of Proton and Electron Auroras in a Substorm', *Geophys. Res. Lett.* **28**, 1139–1142.

Mende, S.B. *et al.*: 2002, 'IMAGE and FAST Observations of Substorm Recovery Phase Aurora', *Geophys. Res. Lett.* **29**, 10.1029/2001GL013027.

Milan, P.T. *et al.*: 2000, 'Dayside Convection and Auroral Morphology During an Interval of Northward Interplanetary Magnetic Field', *Ann. Geophys.* **18**, 436.

Mitchell, D.G. *et al.*: 2001, 'Imaging Two geomagnetic Storms in Energetic Neutral Atoms', *Geophys. Res. Lett.* **28**, 1151–1154.

Mitchell, D.G. *et al.*: 2003, 'Global Imaging of O^+ from IMAGE/HENA', *Space Sci. Rev.*, this issue.

Moore, T.E. *et al.*: 2001, 'Low Energy Neutral Atoms in the Magnetosphere', *Geophys. Res. Lett.* **28**, 1143–1146.

Moore, T.E. *et al.*: 2003, 'Heliosphere-Geosphere Interactions Using Low Energy Neutral Atom Imaging', *Space Sci. Rev.*, this issue.

Newell, P.T. *et al.*: 1989, 'Some Low-Altitude Cusp Dependencies on the Interplanetary Magnetic Field', *J. Geophys. Res.* **94**, 8921.

Pollock, C.J. *et al.*: 2001, 'First Medium Energy Neutral Atom (MENA) Images of Earth's Magnetosphere During Substorm and Storm-time', *Geophys. Res. Lett.* **28**, 1147–1150,

Reinisch, B.W. *et al.*: 2001, 'First Results from the Radio Plasma Imager on IMAGE', *Geophys. Res. Lett.* **28**, 1167–1170.

Sandel, B.R. *et al.*: 2001, 'Initial Results from the IMAGE Extreme Ultraviolet Imager', *Geophys. Res. Lett.* **28**, 1439–1442.

Singh, N., and J. Horwitz: 1992, 'Plasmasphere Refilling: Recent Observations and Modeling', *J. Geophys. Res.* **97**, 1049–1080.

Strangeway, R.J.: 1985, 'Wave Dispersion and Ray Propagation in a Weakly Relativistic Electron Plasma: Implications for the Generation of Auroral Kilometric Radiation', *J. Geophys. Res.* **90**, 9675–9687.

Tsurutani, B.T. *et al.*: 1995, 'Interplanetary Origin of Geomagnetic Activity in the Declining Phase of the Solar Cycle', *J. Geophys. Res.* **100**, 21,717.